Dalton Transactions

An international journal of inorganic chemistry

Accepted Manuscript

Dalton Transactions

An international journal of inorganic chemistry

rsc.li/dalton

Volume 46
Number 10
14 March 2017
Pages 3073-3412

ISSN 0306-0012

COMMUNICATION
Douglas W. Stephen et al
N-Heterocyclic carbene stabilized parent sulfenyl, selenenyl, and tellurenyl cations (XH+; X = S, Se, Te)

ROYAL SOCIETY OF CHEMISTRY

ROYAL SOCIETY OF CHEMISTRY

rsc.li/dalton

Tailoring Supercapacitance and Water Splitting Performance of Nickel Sulfides (NiS and Ni$_3$S$_2$): A Comparative Study of Colloidal and Solventless Synthesis

Gwaza Eric Ayom,[a] Malik Dilshad Khan,[a] Rishabh Srivastava,[b] Wang Lin,[b] Ram K. Gupta[b] and Neerish Revaprasadu[a]*

[a]Department of Chemistry, University of Zululand, Private Bag X1001, KwaDlangezwa 3880, South Africa.

[b]Department of Chemistry, Pittsburg State University, Pittsburg, KS 66762, USA.

*Email: RevaprasaduN@unizulu.ac.za

Dalton Transactions Accepted Manuscript

Abstract

To overcome the potential issue of active site blockage by surfactants in colloidal synthesis, alternative synthetic approaches must be explored. In this study, we investigated both solvent-free and colloidal thermolysis routes to synthesize nickel sulfides (NiS and Ni_3S_2) using sulfur-based Ni complexes, $[Ni(S_2CO(C_2H_5))_2]$ (Ni-Xan) and $[Ni(S_2CN(C_2H_5)_2)_2]$ (Ni-DTC) as precursors. The solvent-free decomposition of these complexes produced ligand-free NiS and Ni_3S_2 in the absence or presence of triphenylphosphine (TPP), respectively. In contrast, colloidal thermolysis in oleylamine (OLA) led to phase-selective nickel sulfide formation (NiS and Ni_3S_2), with TPP facilitating desulfurization. The electrochemical performance of the synthesized materials was evaluated in water splitting and supercapacitance applications. Among the tested materials, NiS synthesized from Ni-Xan in OLA exhibited the highest specific capacitance (809.2 F/g at 1 A/g) and energy density (34.9 Wh/kg), while NiS derived from Ni-DTC in OLA achieved the highest power density (281.7 Wh/kg). Additionally, the Ni_3S_2 electrode obtained via the colloidal route demonstrated superior HER performance, requiring only 197 mV (Tafel slope: 159 mV/dec) to reach a current density of 10 mA/cm^2. These findings underscore that simply eliminating surfactants and adopting a solvent-free method is not inherently sufficient to achieve high electrochemical performance. This study provides insights into the limitations of solvent-free synthesis and outlines potential prerequisites that may guide future optimization for improved electrochemical performance.

Dalton Transactions Accepted Manuscript

Introduction

Energy conversion and storage systems, including water splitting and supercapacitors, are central to the global transition away from fossil fuels. Though fossil fuels have played a crucial role in the industrial development of the planet, their continued usage is associated with environmental challenges such as climate change and pollution.[1, 2] Moreover, carbon-based energy reserves have continually been depleting with use, posing threats to our energy security.[3] Hydrogen has been identified as an ideal substitute for traditional fossil energy sources due to its zero carbon emissions and high energy density.[4-6] The generation of hydrogen/oxygen (hydrogen/oxygen evolution reaction) from water splitting is however restricted by the use of noble metals which improve the reaction kinetics of these thermodynamically challenging processes.[7, 8] The current focus is therefore on the preparation of cheap and readily available alternatives to the exotic metal catalysts for the generation of hydrogen.

Transition metal sulfides continually attract attention as potential substitutes for exotic metals in energy conversion and storage technologies. Nickel sulfides have probably drawn more exploration than other sulfides in sustainable energy technologies.[9] It has been prepared in different compositions, NiS, NiS_2, Ni_3S_2 and N_9iS_8.[10] NiS which has been more documented amongst the nickel sulfide system probably due to thermodynamic stability[11] has been deployed to improve the reaction kinetics of water splitting and in energy storage systems.[9] For example, Zhang *et al.*[12] recently fabricated NiS deploying grapefruit peel and $Ni(NO_3).6H_2O$ as S and Ni precursors, respectively which was applied as an efficient catalyst in HER and OER. We also have reported NiS obtained from metal-organic compounds towards improving the water-splitting reaction kinetics.[10, 13, 14] The relatively scarcer Ni_3S_2 phase is an interesting catalyst due to its electronic structure. It has a rhombohedral structure with tetrahedral nickel atoms giving room for Ni-Ni interactions.[15] These interactions give Ni_3S_2 its metallic behavior which makes it an excellent electrical conductor applicable in catalysis.[16] The Zhong group[17] for example formed Ni_3S_2 using Ni foam and $Na_2S.9H_2O$ which demonstrated high OER activity. Also, nickel sulfides such as Ni_3S_2/NiS[18] and NiS[19] have been employed as electrode materials in supercapacitor fabrication. Nickel sulfides' continued appeal to the research community stems from their abundance in earth reserves,[20] electrical conductivity[17] and versatility in morphology and composition.[10]

The desire for phase-pure nickel sulfides considering the multiplicity of phases in the sulfide system is weighed down by the difficult synthetic protocols. Traditionally, sulfides of

nickel have been prepared by high-temperature decomposition of dual or multiple precursors in the absence of any solvents. For instance, Kosmac and colleagues[21] formed a mixture of nickel sulfide phases by the mechanical alloying of Ni and S powders in a glove box at high temperatures over an extended period. Other solventless synthetic routes like thermal diffusion,[22] solid-to-solid calcination[23] and melt decompositions[10, 24] have also been deployed to fabricate nickel sulfides. These solvent-free routes result not only in poor control of morphology, composition, size and purity of products but also impose high reaction temperatures and time. The use of multiple precursors also makes the synthetic process cumbersome. The colloidal synthetic pathway involving the use of solvents generally yields well-defined particles in terms of dimension, composition and purity.[25] For example, different researchers have employed Ni sources like $Ni(NO_3)_2 \cdot 6H_2O$, nickel acetate tetrahydrate, Ni foam, Ni foil and S providers like thiourea, $Na_2S \cdot 9H_2O$ and 2-mercaptoethanol to fabricate dimensionally controlled and pure Ni_3S_2 and NiS exercising colloidal methods like hydrothermal[17, 26, 27] and solvothermal.[28-30] Also, other routes like microwave-assisted decompositions,[31] electrodeposition[32] and product precipitation[33] have been deployed in the preparation of desired nickel sulfides similarly employing dual or multiple precursors.

The single-source precursor route primarily involving metal-organic frameworks to the formation of nickel sulfides bypasses the challenges associated with the use of multiple precursors. This straightforward and facile route to the fabrication of metal sulfides has been deployed in the synthesis of Ni_3S_2 and NiS. For instance, we have utilized sulfur-based coordination complexes like dithiocarbamates,[34, 35] xanthates[24, 36] and dithiophosphonates[10, 13, 14] to form or deposit nickel sulfides. The use of single-source starting materials or any of the other routes to the formation of nickel sulfides is, however, largely inflexible to the formation of more than one pure phase.

Herein, we utilized xanthate, $[Ni(S_2CO(C_2H_5))_2]$ (Ni-Xan) and dithiocarbamate, $[Ni(S_2CN(C_2H_5)_2)_2]$ (Ni-DTC) complexes to prepare different phases of nickel sulfide (NiS and Ni_3S_2) from a single precursor via a solvent-free and colloidal route. In the solvent-free route, the complexes were pyrolyzed under an inert atmosphere, whereas in colloidal synthesis, oleylamine (OLA) was used as a solvent and capping agent. The study investigates how the choice of starting precursors and the synthetic routes influence the charge storage and water-splitting performance of nickel sulfide phases. This study highlights critical considerations for designing suitable ligands and suggests potential prerequisites that may result in enhancing the performance of materials synthesized via solvent-free routes.

Experimental

Materials

Potassium ethyl xanthogente (96%), sodium diethyldithiocarbamate trihydrate, triphenylphosphine (TPP), nickel chloride hexahydrate, deionized water, chloroform (99.8%), methanol (99.8%) and acetone (99.5%) were purchased from Sigma-Aldrich, Durban, South Africa and used without further purification.

Preparation of nickel complexes

The synthesis of nickel xanthate $[Ni\{S_2CO(C_2H_5)\}_2]$ and nickel dithiocarbamate $[Ni\{S_2CN(C_2H_5)_2\}_2]$ complexes was carried out following previously reported procedures.[14, 36] These complexes were confirmed by elemental analysis. $[Ni\{S_2CO(C_2H_5)\}_2]$: Calc. C, 23.91%; H, 3.35%; S, 42.51%; Ni, 19.49%. Found: C, 23.81%; H, 3.20%; S, 42.17%; Ni, 20.1%. $[Ni\{S_2CN(C_2H_5)_2\}_2]$: Calc. C, 33.62%; H, 6.21%; N, 7.84%; S, 35.90%; Ni, 16.43%. Found: C, 33.73%; H, 6.11%; N, 7.91%; S, 35.79%; Ni, 16.48%.

Preparation of nickel sulfides (NiS and Ni₃S₂) via a solvent-free route

To prepare NiS, 0.2 g of Ni-Xan or Ni-DTC was placed in a ceramic boat and transferred to a quartz tube, which was heated to 250 °C in a furnace under N_2 for an hour. The product was obtained as a black powder and used without any further treatment. The preparation of Ni_3S_2 was similar to that of NiS except that a composite of Ni-Xan (0.10 g, 0.33 mmol) with TPP (0.35 g, 1.32 mmol) or Ni-DTC (0.10 g, 0.28 mmol) with TPP (0.29 g, 1.12 mmol) (i.e. complex to TPP ratio of 1:4 in both cases) was ground before the pyrolysis reactions.

Preparation of nickel sulfides (NiS and Ni₃S₂) in oleylamine

For ligand-capped nickel sulfides, 0.30 g of Ni-Xan or Ni-DTC in olelylamine (5 mL) was placed in a 3-neck flask under N_2 at room temperature and heated slowly to 250 °C and kept at this temperature for 1 hour. The mixture was then allowed to cool to room temperature. The product was isolated as a black powder after two methanol/chloroform (10 mL; 5:1) and two acetone (10 mL) washings to yield NiS. The fabrication of Ni_3S_2 was similar to NiS above except for the homogenization by grinding of Ni-Xan (0.10 g, 0.33 mmol) and TPP (0.17 g, 0.66 mmol) or Ni-DTC (0.10 g, 0.28 mmol) and TPP (0.22 g, 0.84 mmol) before thermolysis in oleylamine.

Instrumentation

Elemental analysis of complexes Ni-Xan and Ni-DTC was obtained from a PerkinElmer CHN analyzer (2400 series II). Thermogravimetric analysis (TGA) was done using a Mettler-Toledo TGA/DSC instrument. The TGA analysis was done in an inert atmosphere (N_2) at a heating rate of 10 ℃ per minute. Powder X-ray diffraction patterns of the fabricated nickel sulfides were acquired from a Bruker D8 Diffractometer with a CuKα radiation source. The patterns obtained were compared to standard diffraction patterns from the International Centre for Diffraction Data (ICDD). Transmission electron microscopy (TEM) images of the formed materials were acquired from a JEOL TEM instrument (1400). Sample preparation for TEM involved dropping the diluted solution of the desired material onto Formvar-coated grids. The coated grids were left to dry at room temperature and then viewed for TEM at 120 kV. TEM images were analyzed via iTEM software. Scanning electron microscopy (SEM) investigations were carried out on Philips XL30 FEG-SEM while those for energy-dispersive X-ray spectroscopy (EDX) were performed with the same instrument that was equipped with a DX4 detector. X-ray photoelectron spectroscopy (XPS) was carried out to examine the surface chemistry via a Thermo ESCAlab 250 Xi spectrometer equipped with a monochromatic AI kα X-ray source.

Electrochemical studies

Electrochemical investigations of the formed nickel sulfides were performed using a Versastat 4-500 workstation from Applied Research, USA which deployed a three-electrode system. Nickel foams (MTI Corporation, USA, 99.99% purity) were employed as electrodes' substrates. Sample preparation for these examinations was carried out by forming pastes of the nickel sulfides using (80 wt%), polyvinylidene difluoride (PVDF, 10 wt.%), and acetylene black (10 wt.%), which was prepared using N-methyl pyrrolidinone (NMP). The as-prepared paste was then applied to nickel foams which were pre-cleaned and weighed, and used as working electrodes. Platinum wire and saturated calomel electrode (SCE) were used as counter and reference electrodes, respectively. Supercapacitance investigations of synthesized materials were performed using a 3 M KOH electrolyte. Charge storage capacity was determined using cyclic voltammetry (CV), galvanostatic charge-discharge (GCD) and electrochemical impedance spectroscopy (EIS) at varying scan rates and current densities. The electrocatalytic properties of fabricated electrodes were analyzed by CV and linear sweep voltammetry (LSV).

Results and discussion

Synthetic procedures for the synthesis of the sulfur-based complexes; xanthates and dithiocarbamates, are well documented.[14, 36] The preparation of Ni-Xan and Ni-DTC followed these standard protocols. The thermal stability and decomposition profile of the complexes, TPP and the composite of the complexes with TPP are shown in **Figure S1**.[13, 14, 36] In brief, Ni-Xan and Ni-DTC show moderate thermal stability with decomposition between 150 to 230 °C resulting in NiS residues. TPP decomposes cleanly without any residue and the composites Ni-Xan/TPP and Ni-DTC/TPP decompose at lower temperatures in comparison to their relative single parent complexes.

The solvent-less pyrolysis of Ni-Xan/TPP and Ni-DTC/TPP in an inert atmosphere (N_2) at 250 °C for an hour yielded hexagonal NiS. The formation of phase-pure NiS (ICDD# 01-075-0613) for Ni-Xan (NiS-3) and Ni-DTC (NiS-4) was confirmed by the powder XRD as matched to the standard reference patterns [**Figure 1(i)**]. The facile formation of phase-pure NiS from these precursors is anticipated since nickel is directly bonded to the sulfur in the complexes and their thermal decomposition has been reported to lead to volatile components that are easily removable.[36, 37] The solvent-free preparation of NiS from Ni-Xan and Ni-DTC is not only straightforward but also scalable. We also explored the fabrication of nickel sulfides from both complexes mediated by TPP via the solvent-free pyrolysis route. This procedure requires the initial homogenization of the desired amounts of TPP with Ni-Xan or Ni-DTC before the pyrolysis reactions. The decomposition of the composite of Ni-Xan with TPP (1:4) at 250 °C for 1 hour under an N_2 atmosphere afforded phase-pure nickel sulfide which matched well to heazlewoodite Ni_3S_2 (Ni_3S_2-2) of the rhombohedral crystal system as per the ICDD# 01-085-0775 [**Figure 1(iii)**]. Similarly, the pyrolysis of Ni-DTC with TPP (1:4) under the same conditions afforded phase-pure heazlewoodite Ni_3S_2 (ICDD# 01-085-0775) which will be referred to as Ni_3S_2-4. It is noteworthy that the stoichiometry of the metal complex precursor to TPP in these decomposition reactions is crucial for the successful fabrication of Ni_3S_2. For instance, the pyrolysis of a 1:3 composite of Ni-DTC with TPP yielded a mixture of nickel sulfides identified as rhombohedral Ni_3S_2 (ICDD# 01-073-0698) and orthorhombic Ni_9S_8 (ICDD# 01-078-1886) as shown in **Figure S2**. Though the Ni_3S_2 material is highly desired due to its excellent catalytic activity,[38, 39] synthetic protocols have been largely limited to the colloidal routes.[15, 40] In addition, dual or multiple precursors have dominated the colloidal

pathway to Ni_3S_2 fabrication hence their formation procedures are usually complex and time-consuming.[40] Therefore, the use of cheap, readily available, and chemically stable TPP to mediate the solvent-free formation of Ni_3S_2 from single-source precursors offers a significant advantage over conventional methods.
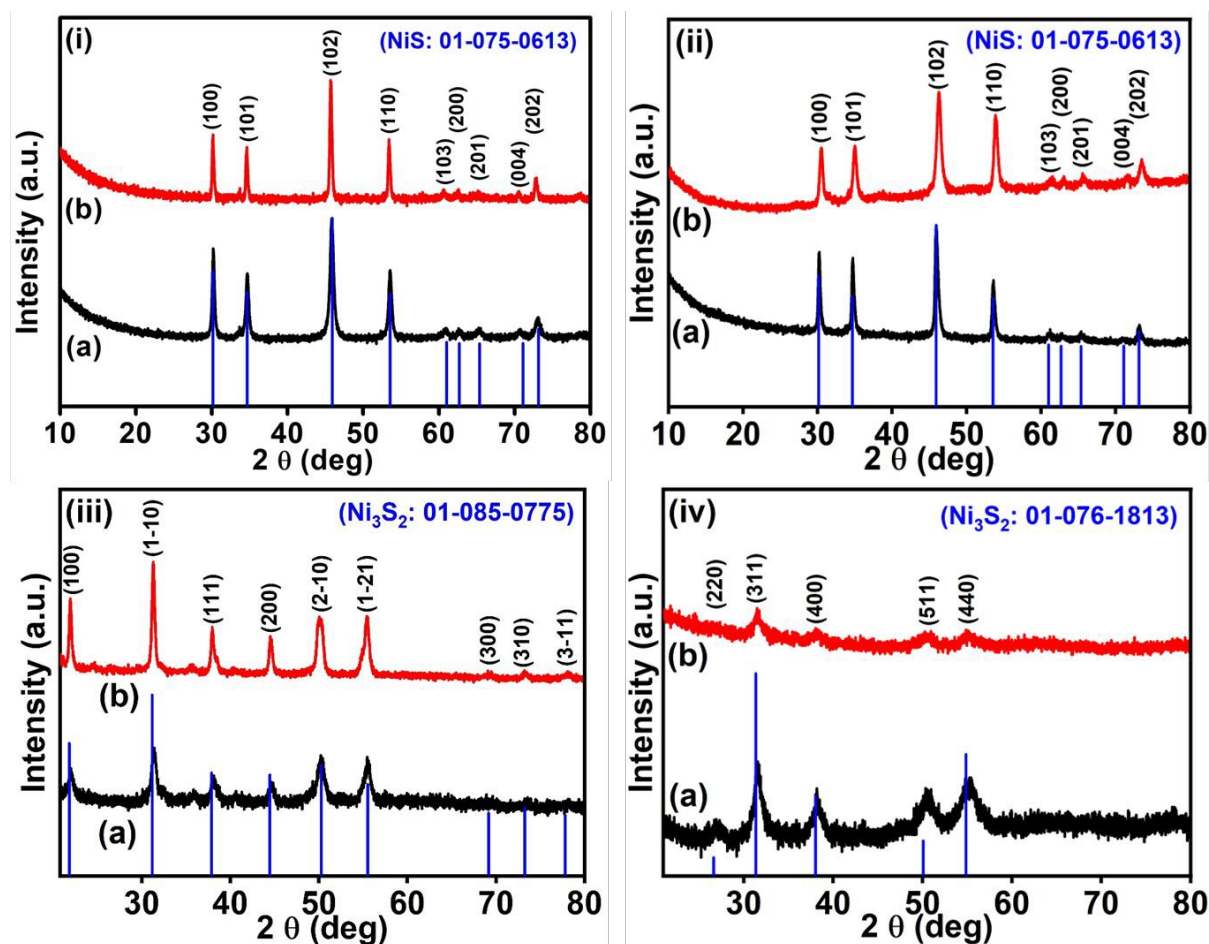
Figure 1. p-XRD patterns of the decomposition of Ni complexes (a) Ni-Xan or (b) Ni-DTC via the (i) solvent-less and (ii) colloidal routes. p-XRD patterns of the decomposition of the composites (a) Ni-Xan/triphenylphosphine or (b) Ni-DTC/triphenylphosphine via the (iii) solventless and (iv) colloidal routes.

Similar reactions were also carried out via a colloidal method to gain further insight into the role of TPP in this formation of nickel sulfides. The decomposition of Ni-Xan (NiS-1) or Ni-DTC (NiS-2) in oleylamine (OLA) by the heat-up protocol at 250 ºC for 1 hour formed nickel sulfide which matched well with hexagonal NiS (ICDD# 01-075-0613), as shown in **Figure 1(ii)**.

Table 1 summarizes the precursors, experimental conditions, phases obtained, and codes used in this study as well as the average crystallite sizes of the synthesized catalysts.

Table 1. Summary of precursors, synthetic route & conditions and phases obtained.

Complexes/Composites	Synthetic route	Reaction conditions	Phase formed	Code	Average crystallite size (nm)
$[Ni\{S_2CO(C_2H_5)\}_2]$ (Ni-Xan)	Colloidal	250 °C, in oleylamine, 1 hr	NiS	NiS-1	33 ± 5
$[Ni\{S_2CN(C_2H_5)_2\}_2]$ (Ni-DTC)	Colloidal	250 °C, in oleylamine, 1 hr	NiS	NiS-2	22.5 ± 4
$[Ni\{S_2CO(C_2H_5)\}_2]$ (Ni-Xan)	Solventless	250 °C, 1 hr	NiS	NiS-3	23 ± 7
$[Ni\{S_2CN(C_2H_5)_2\}_2]$ (Ni-DTC)	Solventless	250 °C, 1 hr	NiS	NiS-4	49 ± 3
$[Ni\{S_2CO(C_2H_5)\}_2]$ (Ni-Xan)/triphenylphosphine (**TPP**)	Colloidal	250 °C, in oleylamine, 1 hr	Ni_3S_2	Ni_3S_2-1	12 ± 8
$[Ni\{S_2CO(C_2H_5)\}_2]$ (Ni-Xan)/ triphenylphosphine (**TPP**)	Solventless	250 °C, 1 hr	Ni_3S_2	Ni_3S_2-2	16 ± 2
$[Ni\{S_2CN(C_2H_5)_2\}_2]$ (Ni-DTC)/ triphenylphosphine (**TPP**)	Colloidal	250 °C, in oleylamine, 1 hr	Ni_3S_2	Ni_3S_2-3	26 ± 14
$[Ni\{S_2CN(C_2H_5)_2\}_2]$ (Ni-DTC)/ triphenylphosphine (**TPP**)	Solventless	250 °C, 1 hr	Ni_3S_2	Ni_3S_2-4	28 ± 8

There are limited reports on the fabrication of NiS in OLA via the heat-up method employing single-source precursors and mostly involving using a combination of solvents or additives.[41-44] The preparation of NiS in OLA as presented is facile and straightforward. The thermolysis of composites of Ni-Xan or Ni-DTC with TPP in OLA, formed Ni_3S_2 just like the solvent-less pyrolysis reactions. The synthetic protocol for these reactions entailed the initial homogenization of the required complex and the desired amount of TPP by grinding before

decomposition in OLA by the heat-up method at 250 ℃ for 1 hour under N_2. The thermolysis of the composite of Ni-Xan and TPP in 1:2 stoichiometry resulted in Ni_3S_2 (Ni_3S_2-1) of the cubic crystal system as per (ICDD# 01-076-1813) as shown in **Figure 1(iv)**. Similarly, the decomposition of Ni-DTC/TPP (1:3) in OLA at 250 ℃ resulted in nickel sulfide, which matched well with Ni3S2 (ICDD# 01-076-1813), referred to as Ni_3S_2-3, as shown in Table 1. The stoichiometry of the complex to TPP is critical in the formation of Ni_3S_2 in the colloidal route just like in the solvent-free pyrolysis path stated above. For example, the thermolysis of Ni-DTC/TPP (1:2) in OLA at 250 ℃ yielded a mixture of nickel sulfides that matched rhombohedral NiS (ICDD# 01-086-2280) and the non-stoichiometric hexagonal $Ni_{0.96}S$ (ICDD# 00-050-1791) as shown in **Figure S3**. It is worth noting that the colloidal synthesis of Ni_3S_2 is often carried out using dual or multiple precursors and typically relies on the time-intensive hydrothermal route.[40] In our previous work, we reported the use of single-source precursors in colloidal synthesis with trioctylphosphine (TOP) to obtain the Ni_3S_2 phase and proposed the role of TOP in achieving a sulfur-deficient composition.[35, 45] The use of single-source precursors and the heat-up method in preparing Ni_3S_2 simplifies most documented protocols.

The role of TPP in the formation of Ni_3S_2 by colloidal as well as solvent-free routes employing sulfur-based coordination complexes is interesting and needs further probing. Trialkylphosphines have been used as desulfurization agents as well as a source of phosphorus for metal phosphide formation. For example, colloidal or solvent-less thermolysis of various chalcogen-based metal-organic precursors in the presence of trialkyl/arylphosphines at high temperatures resulted in the formation of metal phosphide nanomaterials.[10, 13, 14, 46, 47] In addition, they have been used for the desulfurization of metal chalcogenides to yield metallic (Ag, Sb, Bi) or bi-/intermetallic (AgBi, Ag_3Sb) compounds.[48-50] TPP therefore mediates the formation of the non-stoichiometric Ni_3S_2 in solvent-free and colloidal routes by partial desulfurization. The partial desulfurization by TPP also explains the formation of the sulfur-rich $Ni_{0.96}S$ phase for the lower TPP composite amount (Ni-DTC/TPP; 1:2) compared to the sulfur-deficient Ni_3S_2 (Ni-DTC/TPP; 1:3) in the colloidal decompositions of Ni-DTC/TPP composite (**Figures 1 & S3**). The mediating role of trialkylphosphines in the formation of functional materials can therefore be explored to prepare desirable but scarcely available metal chalcogenide analogues.

The microstructure of the formed NiS and the TPP-assisted fabricated Ni_3S_2 via the solvent-less and colloidal routes were examined by employing scanning electron microscopy (SEM), energy-dispersive X-ray (EDX), transmission electron microscopy (TEM) and selected

area electron diffraction (SAED). The SEM images of the nickel sulfides indicate agglomerated particles without any defined shape at such low magnification (**Figures 2 & S4**). However, Ni_3S_2 particles obtained in OLA (**Figure 2c**) and the NiS and Ni_3S_2 formed from the solvent-less pyrolysis of complex **2** (**Figures S4b,d**) showed sheet-like morphologies.

TEM analysis of nickel sulfides provided further insight into these materials' microstructure. The TEM images (**Figures 3 & S5**) of the prepared sulfides confirm the agglomeration and compact arrangement of the particles. It also revealed that these materials have a non-uniform morphology consisting of spherical and elongated-shaped particles. The elemental mapping images of the fabricated sulfides indicate exclusively the presence of Ni and S which were well distributed as shown in **Figures 2 & S3**. Also, the experimental atomic percentage composition (EDX) of nickel sulfides agreed with the theoretical values (**Table S1**).
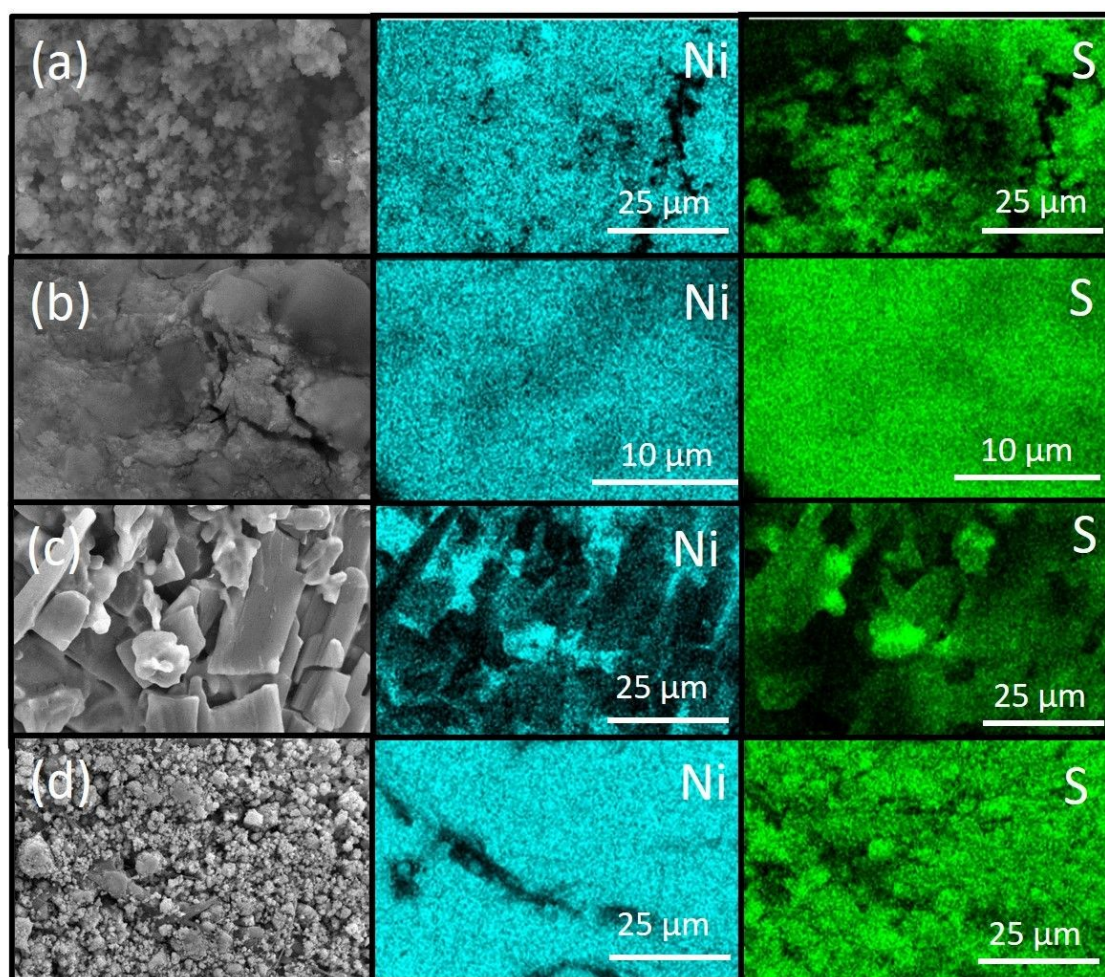

Figure 2. SEM images of NiS obtained from the decomposition of (a) Ni-Xan and (b) Ni-DTC and Ni_3S_2 obtained from the decomposition of (c) Ni-Xan/TPP and (d) Ni-DTC/TPP all in OLA.

Figure 3. TEM images of NiS obtained from the decomposition of (a) Ni-Xan and (b) Ni-DTC and Ni_3S_2 obtained from the decomposition of (c) Ni-Xan/TPP and (d) Ni-DTC/TPP, all in OLA and their (e-h) respective SAED and (i-l) HRTEM images.
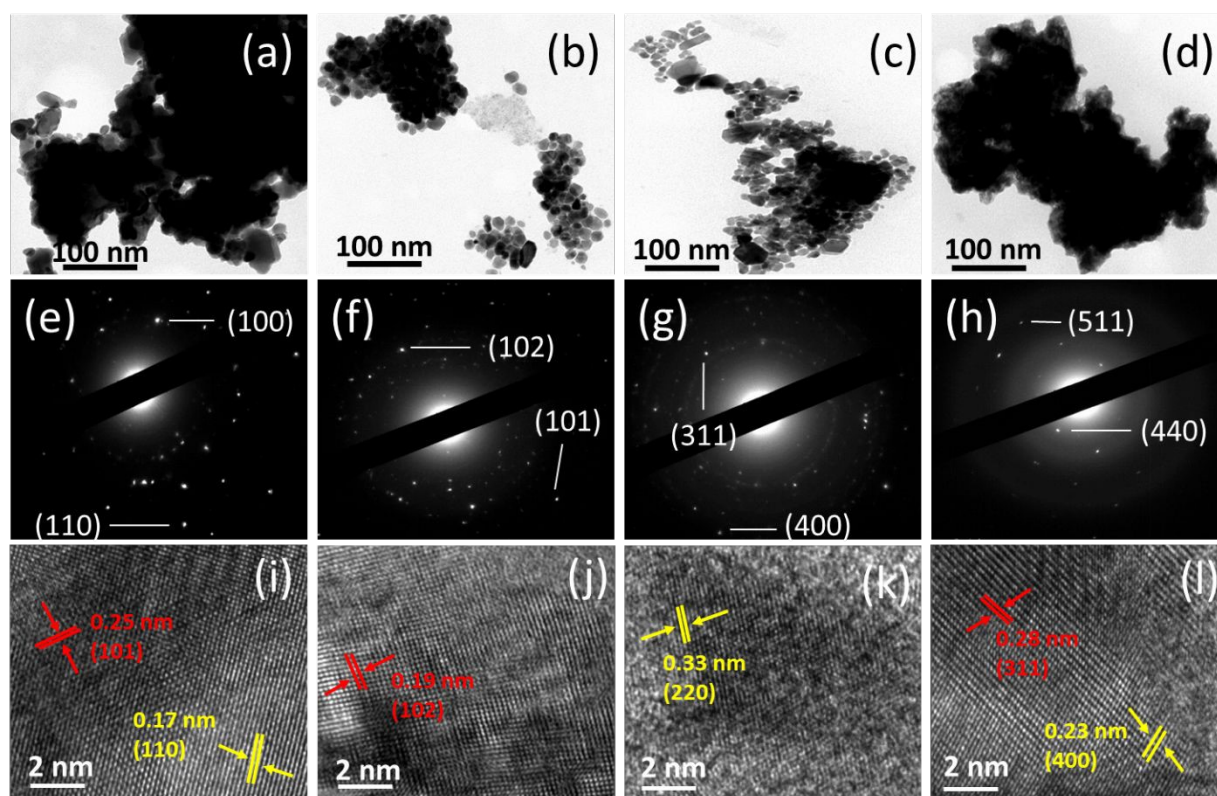
The crystallinity of the formed materials was examined by SAED and HRTEM analysis (**Figures 3 & S5**). SAED images show well-defined spots that match well per respective XRD and ICDD standard patterns, indicative of good crystallinity. The SAED results were affirmed by the clear lattice fringes of the formed sulfides that were in agreement with the standard patterns, as shown in the HRTEM results. We also calculated the crystallite size of our formed sulfides from our XRD results via the Debye–Scherrer equation ($L = \frac{0.89\lambda}{\Box cos\theta}$; L = sulfide's average crystallite size, λ = X-ray wavelength, $\Box$ = full width at half maximum, and θ = Bragg's angle) to check the effect of the synthetic route on particle size as given in **Table 1**. NiS particles from the colloidal route were relatively smaller and less agglomerated than those from the solventless method, due to better morphology control and surface capping by the solvent (**Figs 3 & S4**). Likewise, pure NiS made without TPP was larger than TPP-containing Ni_3S_2, indicating TPP's role as a capping agent that limits particle growth.

X-ray photoelectron spectroscopy (XPS) spectra of the formed and transformed sulfides were employed to examine the surface chemistry of our materials (**Figs 4 & S6**). The survey spectrum of the colloidally formed NiS (NiS-1) indicated a composition of Ni, S, C, O and N. Apart from the expected Ni, S and residual C, O and N were attributed to surface oxidation and the capping amine group (OLA), respectively. The deconvoluted Ni 2p peaks at 855.2 and 873.2 eV (**Fig. 4b**) are assigned to $2P_{3/2}$ and $2p_{1/2}$, respectively, characteristic of Ni^{2+} of the sulfide.[51, 52] Additional Ni 2p peaks at 852.5 and 869.4 eV are assigned to Ni^+ and metallic Ni^0 while the satellite peak at 860.8 and shakeup peak at 878.8 eV are typical of nickel.[51] The S 2p region showed two peaks (**Fig. 4c**), including 160.8 ($2p_{3/2}$) and 162.2 eV ($2p_{1/2}$) attributed to S of the sulfide. Other regions with peaks at 398.8, 284.4 and 530.7 eV (**Fig. 4d & S6Ib,c**) are assigned to N, C and O, respectively. The colloidally transformed sulfide (Ni_3S_2-2) had similar XPS results as expected (**Fig. 4e- I & SId-f**) with the presence of the P 2p region, the major exception (**Fig. 4i**). The peaks at $2p_{3/2}$ (129.2) and $2p_{1/2}$ (132.7 eV) are typical of metal phosphides and are due to residual amorphous nickel phosphide formed in the transformation of NiS to Ni_3S_2.[53] Also, all the deconvoluted XPS regions of Ni_3S_2-2 had slightly higher binding energies compared to NiS-1, indicative of phase transformation.
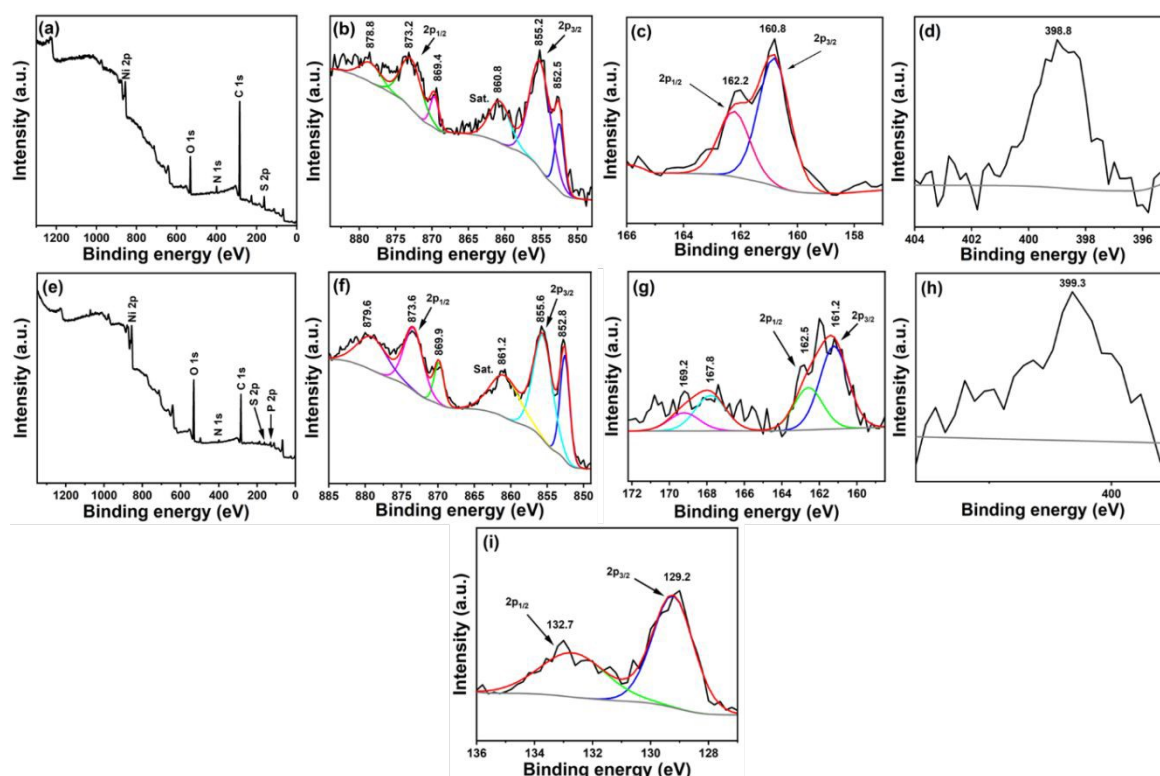

Figure 4. XPS spectra of formed sulfides. Survey spectrum (a) and Ni 2p (b), S 2p (c) N 1s regions of NiS-1. Survey spectrum (e) and Ni 2p (f), S 2p (g) N 1s (h), P 2p (i) regions of Ni_3S_2-1.

The XPS analysis of the solventless formed sulfides (**Fig S6II**) is similar to the ones from the colloidal route except for the absence of the N 1s region since no solvents were employed. The minor P 2p signal observed in the XPS spectrum, in all the transformed sulfides, i.e. Ni_3S_2 as given in **Figs 4 & S6**, may originate from residual TPP or surface-bound phosphorus-containing intermediate species formed during the phase transformation.

Electrochemical properties of formed nickel sulfides for supercapacitor applications

Supercapacitance studies were conducted to evaluate the electrochemical performance of the as-synthesized materials. The results suggest that the obtained materials are promising candidates to bridge the function of dielectric capacitors with high power density.[54] The electrochemical activity, capacitive performance and feasibility of charge transfer were comprehensively investigated via cyclic voltammograms (CV) in 3 M KOH in various cycles at different scan rates ranging from 2 mV/s to 300 mV/s in a potential window of 0.0-0.6 V as shown in **Figures 5 & S7**. Henceforth, the NiS formed from the decomposition of complexes Ni-Xan and Ni-DTC in OLA will be referred to as NiS-1 and NiS-2 while the ones obtained from the solvent-less pyrolysis of these complexes will be denoted as NiS-3 and NiS-4, respectively. Similarly, Ni_3S_2 fabricated from the composites of Ni-Xan and Ni-DTC with TPP in the colloidal route will herewith be known as Ni_3S_2-1 and Ni_3S_2-2 while those obtained via the solvent-free method will be Ni_3S_2-3 and Ni_3S_2-4, respectively (**Table 1**). The CV results show a set of non-rectangular-shaped redox peaks suggestive of the pseudocapacitive behavior of synthesized materials.[55] The shape of the CV curves for all the electrodes was maintained at low and high scan rates, resembling a quasi-reversible reaction due to multiple valence states of the Ni such as Ni^0/Ni^{2+}, Ni^0/Ni^{3+} and Ni^{2+}/Ni^{3+} indicative of its fast charge-discharge ability. The deduced faradic redox reaction for the NiS and Ni_3S_2 materials are shown in **equations 1 and 2**.[56, 57]

$$NiS + OH^- \leftrightarrow NiSOH + e^- \qquad \textbf{(1)}$$

$$Ni_3S_2 + 3OH^- \leftrightarrow Ni_3S_2(OH)_3 + 3e^- \qquad \textbf{(2)}$$
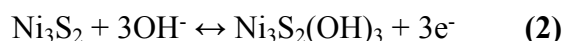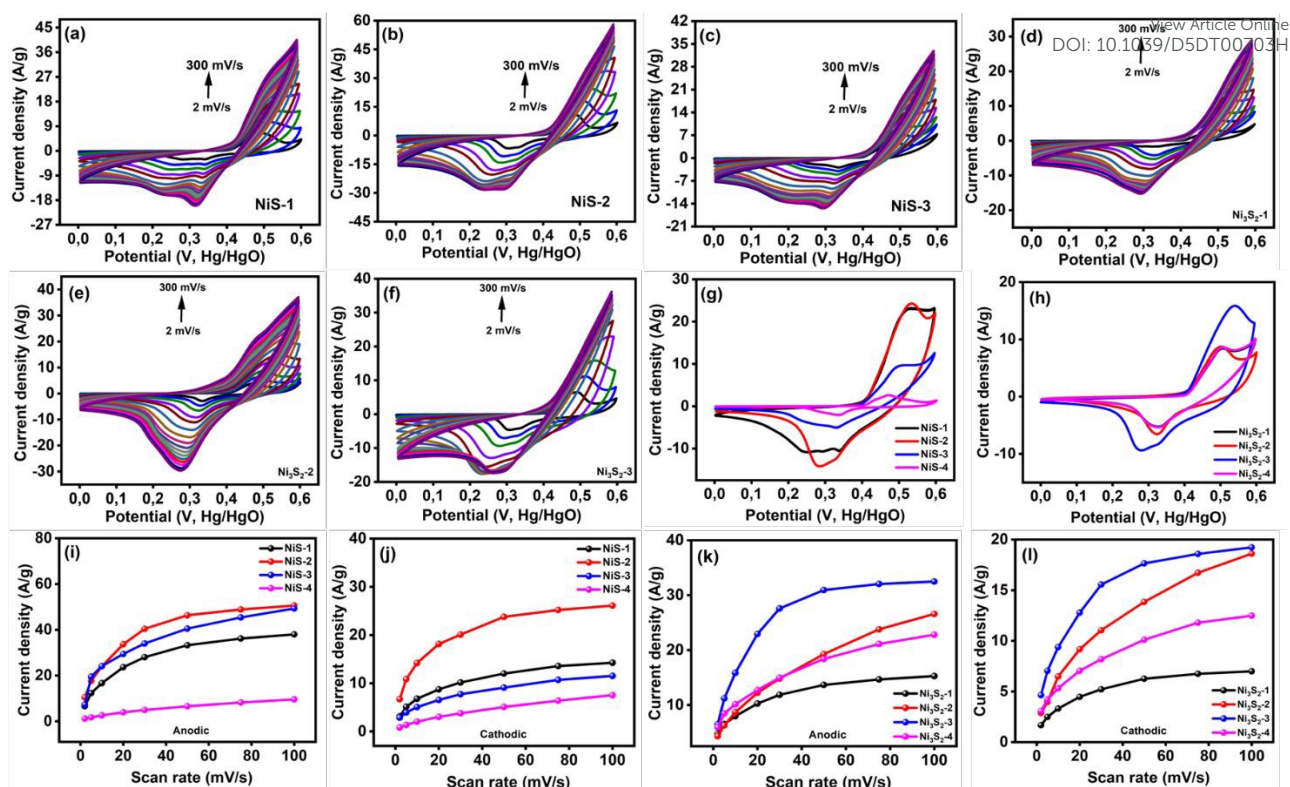
Figure 5. (a-c) CV voltammograms for the NiS electrodes and (d-f) for the Ni₃S₂ samples. (g) CV comparison for the NiS electrodes and (h) for the Ni₃S₂ ones all at a scan rate of 10 mV/s. Current density vs scan rate for (i) anodic, (j) cathodic regime for the NiS materials and (k) anodic and (l) cathodic regime for the Ni₃S₂ electrodes.

To gain further insight into the charge transfer kinetics of these materials, a comparison of the CV curves for the NiS and Ni₃S₂ samples at a scan rate of 10 mV/s was delineated as shown in **Figure 5g,h**. These comparative curves clearly show that among the NiS and Ni₃S₂ samples, NiS-1, NiS-2 and Ni₃S₂-3 have more enclosed areas which are a pointer to their superior electrochemical kinetics. Also, the anodic potential (E_a) and cathodic potential (E_c) of the samples were noted where NiS-1 and NiS-2 had lower differences between E_a and E_c compared to Ni₃S₂-1 and Ni₃S₂-2, all formed via the colloidal route. On the other hand, the samples obtained via the solvent-free method showed a different result. Here, Ni₃S₂-3 and Ni₃S₂-4 showed higher peak potential differences than NiS-3 and NiS-4. It is important to note that the lower potential difference between the peaks shows better electronic transmission movement and ion fusibility due to low charge transfer resistance. NiS-2 and Ni₃S₂-3 offered the least ion resistance among the electrodes and hence amplified ion mobility suggestive of better charge storage capacity among all the electrodes. It is important also to note that lower potential difference means faster redox processes which also enrich the power density and energy density of a material.

The anodic and cathodic peak current density of the electrodes was plotted to the scan rate as shown in **Figure 5i-l** to probe into the charge storage capacity of nickel sulfides. No linear correlation between the anodic and cathodic peak current density as a function of scan rate is observed for all the electrodes indicating that charge storage has pseudocapacitance characteristics and not an absorption mechanism which is in agreement with the CV results. The charge storage mechanism for all the electrodes was probed further using the Sevcik equation.[58] The linear plots of the current density vs the scan rates for all the electrodes indicated diffusion-assisted mechanism of the electrochemical oxidation and reduction processes as shown in **Figure 6a-d**. The linear fitting of these plots resulted in the highest anodic slope of 4.81 for NiS-2 (**Figure 6a**) among all the NiS samples whereas for the Ni_3S_2 electrodes, Ni_3S_2-3 had the highest slope of 3.03 (**Figure 6b**). These results suggest that NiS-2 and Ni_3S_2-3 electrodes with faster oxidation processes have the best storage capacity with the highest rate of permeation of ions compared to their regression rate. Furthermore, cathodic intercepts were also plotted as shown in **Figure 6c,d** with NiS-2 and Ni_3S_2-3 similarly having the better reduction processes (i.e. the slopes and intercepts). NiS-2 (prepared by the colloidal route) and Ni_3S_2-3 (obtained by the solvent-less protocol) therefore show the best charge transfer rate and storage capability potentials compared to all the electrodes.

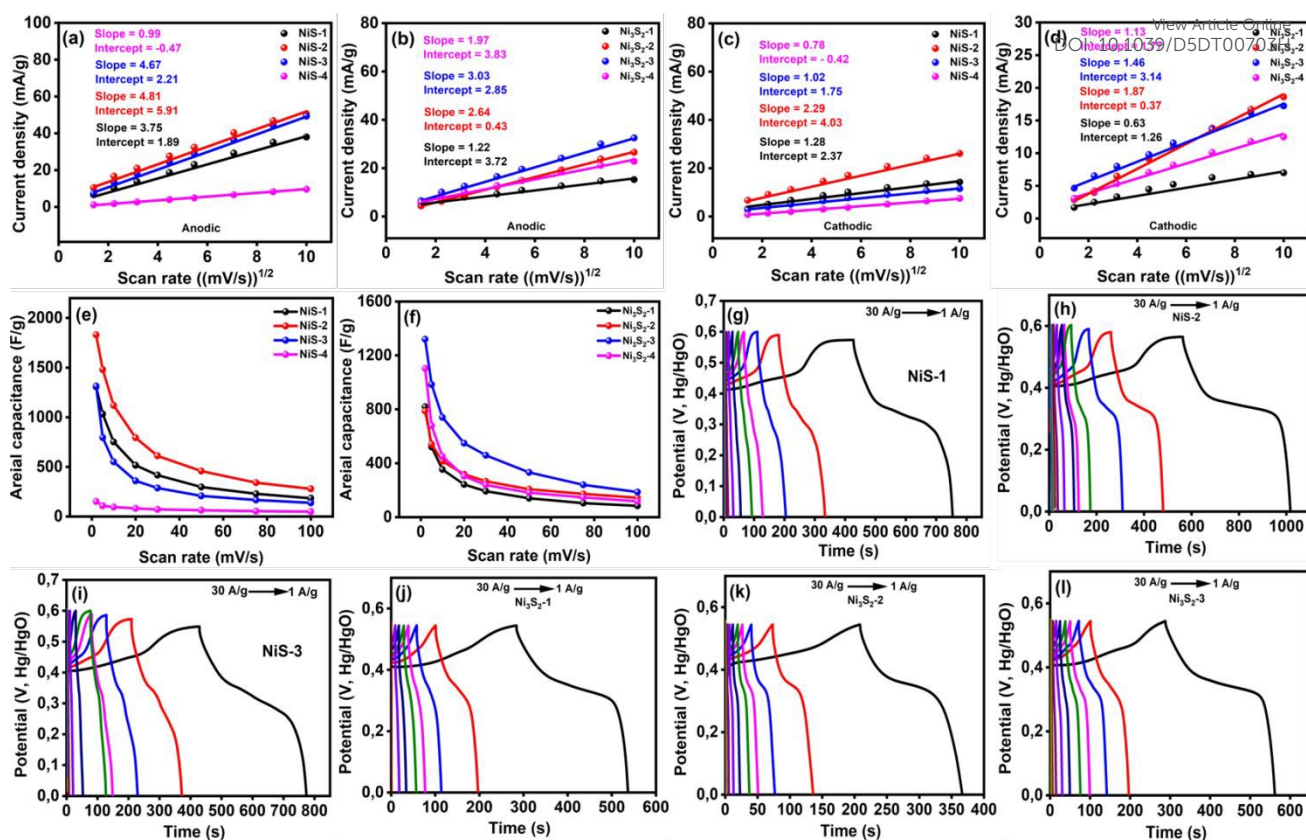**Dalton Transactions Accepted Manuscript**

Figure 6. Current density vs square root of scan rate at the anodic regime for (a) the NiS electrodes and (b) for the Ni_3S_2 ones. The corresponding cathodic regime for (c) the NiS electrodes and (d) the Ni_3S_2 ones. Specific capacitance obtained from the CV for (e) the NiS samples and (f) the Ni_3S_2 ones. GCD curves for the electrodes (h-l).

The specific capacitance of the samples was calculated using the CV curves employing **equations 3 & 4**:[59]

$$\int_{V1}^{V2} I(V)dv = \int_{V1}^{V2}(C_p * m * k)dv \qquad (3)$$

$$C_p = \frac{A}{2ka\Delta V} \qquad (4)$$

where I (V) denote current, Δv is the potential window, Cp is the calculated gravimetric specific capacitance (F/g) and A (cm^2) is the area under the CV curve. K (Vs^{-1}) is the scan rate of the CV and a (cm^2) is the area of the sample on Ni foam. The calculated capacitance at various scan rates is shown in **Figure 6e,f**. As expected NiS-2 and Ni_3S_2-3 had the highest calculated specific capacitance of 1900 and 1400 F/g, respectively. These results compare well to the capacitance of recently formed nickel sulfides. For instance, $Ni_{0.5}Co_{0.5}S$ (1512 F/g),[60] NiS-Sn (732 F/g)[61] and Ni_3S_2 (610 F/g)[62] had comparative or lower capacitance at 1 mVs-1, 1 A/g and 0.5 A/g respective current densities (**Table S2**). Furthermore, the galvanostatic charge-

17

discharge (GCD) curves were employed to check the charging and discharging behavior of the as-synthesized materials for supercapacitor application at a potential window of 0.0-0.6 V for NiS electrodes and 0.0-0.57 V for the Ni_3S_2 ones at varying current densities in a 3 M KOH solution (**Figures 6g-l & S8**). The non-linear GCD curves observed for all the materials indicate their redox nature which agrees with the CV results. Generally, discharge time increases with decreasing current density suggestive of improved storage capacity even at lower current densities. NiS-2 (prepared by the colloidal route) and Ni_3S_2-3 (formed by the solvent-less protocol) by the GCD curves had the best charge-discharge time which aligns with the CV results.

The specific capacitance (C_s) of the electrodes was also calculated by the following **equation 5** using GCD measurements.

$$C_s = I*\Delta t/(m*\Delta V) \qquad (5)$$

Herein, C_s is the specific capacitance (F/g), I is the current (A), Δt is the discharge time (s), m is the mass of the active material (g) and ΔV is the potential window. From the calculated results the specific capacitance vs current density plots for all the electrodes were done and are shown in **Figure S9a,b**. NiS-2 as expected showed the highest specific capacitance of 809.2 F/g compared to NiS-1 & NiS-3 (with an average of 600 F/g) and NiS-4 (50 F/g) at 1 A/g of current density. For the Ni_3S_2 electrodes, the ones prepared by the solvent-less route (Ni_3S_2-3 & Ni_3S_2-4) had the best specific capacitance (about 500 F/g) in comparison to the samples formed by the colloidal method (Ni_3S_2-1 & Ni_3S_2-2) with 300 F/g at the current density of 1 A/g. Therefore, the specific capacitance of the NiS samples formed by the colloidal method and the Ni_3S_2 ones fabricated by the solvent-free protocol was better than the respective other electrodes. The energy storage capacity of synthesized materials compares well with other recently documented Ni-based electroactive materials as shown in **Table S2**.

Since the energy and power density of a capacitor are crucial to estimating its practical application, they were calculated using **equations 6 and 7**:[63]

$$E = 0.5CV^2 \text{ (Wh/kg)} \qquad (6)$$
$$P = 3.6*E/\Delta t \text{ (kW/kg)} \qquad (7)$$

where C is the specific capacitance (F/g), V is the voltage window, and Δt is the discharge time obtained from GCD. The energy and power density of NiS-1, NiS-2, NiS-3, and NiS-4 were calculated as 25.5, 34.9, 25.7 and 2.3 Wh/kg, and 281.7, 278.2, 268.1 and 277.6 kW/kg, respectively. On the other hand, the energy and power density of Ni_3S_2-1, Ni_3S_2-2, Ni_3S_2-3,

Dalton Transactions Accepted Manuscript

and Ni_3S_2-4 are 11.4, 11.7, 20.3, and 18.7 Wh/kg, and 261.5, 267.3, 267.3 and 266.4 kW/kg respectively. The energy density of the NiS electrodes was better than that of the Ni_3S_2 ones with the NiS-2 (prepared by the colloidal route) having the best result which agrees with the capacitance performance. On the other hand, among the Ni_3S_2 electrodes, Ni_3S_2-3, obtained via solvent-free method as expected showed the best energy density values. Also, all the nickel sulfide electrodes (both NiS and Ni_3S_2) had similar power density results as shown in **Figure S9c,d**.

The electrochemical stability of an energy storage device is another key pointer towards its practical application and was evaluated through the cycling processes. The coulombic efficiency of two best-performing electrodes was evaluated in terms of energy storage i.e. NiS-2 and Ni_3S_2-3 as shown in **Figure S9e,f**. NiS-2 and Ni_3S_2-3 remarkably showed 100% coulombic efficiency over 5000 cycles indicative of cycling stability. NiS-2 and Ni_3S_2-3 electrodes also showed exceptional capacitance retention of 91.3% and 80.2%, respectively over 5000 cycles of testing. Therefore, energy storage testing parameters like CV, electrochemical kinetics, and capacitance derived using CV area and that obtained by GCD evaluations collectively indicate that colloidally prepared NiS and solvent-free formed Ni_3S_2 with NiS-2 and Ni_3S_2-3 materials showed the best performance among all the electrodes. This then means that the high carbon content of the solventless prepared NiS limited its energy storage performance more than the OLA capping agent blocking the active sites. Contrarily, OLA's adsorption on Ni_3S_2 had less of a negative impact on its storage functionality compared to the carbon content.

Electrocatalytic properties of formed nickel sulfides for water-splitting applications

We also investigated the electrocatalytic characteristics of fabricated nickel sulfides in water splitting. Though water splitting holds a lot of promise in hydrogen generation, these reactions are constrained in high thermodynamics necessitating the use of catalysts.[64] The HER performance of the materials was evaluated in a three-electrode system in 1 M KOH via linear sweep voltammetry (LSV) and Tafel slopes (**Figure 7**). NiS-1, NiS-2, NiS-3 and NiS-4 electrodes needed 225, 233, 247 and 240 mV to reach 10 mA/cm^2 current density alongside Tafel slopes of 158, 147, 152 and 147 mV/dec, respectively. NiS-1 was therefore the best catalyst among the NiS materials in reducing the constraining overpotential, while NiS-2 and NiS-4 had the fastest reaction kinetics. Similarly, Ni_3S_2-1, Ni_3S_2-2, Ni_3S_2-3, and Ni_3S_2-4 required overpotentials and Tafel slopes of 230, 197, 240 & 245 mV and 156, 159, 160 & 152 mV/dec, respectively, to attain the same current density. Pt/C, the state-of-the-art HER catalyst,

had the best performance as expected with 31 mV at 10 mA/cm^2. The Ni_3S_2-2 material was therefore the best performing in HER among all electrodes with Ni_3S_2-4 having the fastest reaction kinetics within the Ni_3S_2 electrodes. Ni_3S_2 is structurally made up of Ni_3-atoms connected by Ni-Ni bonds, providing good electrical conductivity.[15] Moreover, the incorporation of phosphorus into Ni_3S_2 has been shown to enhance its catalytic performance.[65] These could explain the good performance of the Ni_3S_2-2 sample in HER. The HER performance of nickel sulfide materials compares well with or outperforms similar electrodes documented in the literature (**Table S3**).

The performance of all materials towards OER was also investigated in an alkaline environment. Rare earth and exotic elemental oxides like IrO_2 and RuO_2 are the benchmark catalysts for OER, which restricts the practical application of these technologies. Readily available substitutes like nickel sulfides are therefore highly sought after. The OER performance of the fabricated electrodes was examined by polarization curves, as shown in **Figure 7**. To attain 10 mA/cm^2 current density, Ni_3S_2-1, Ni_3S_2-2, Ni_3S_2-3 and Ni_3S_2-4 required 275, 298, 272, 256 mV with Tafel slopes of 73, 66, 88 and 71 mV/dec, respectively. Also, the NiS samples needed overpotentials/Tafel slopes of 257/81 (NiS-1), 257/72 (NiS-2), 267/90 (NiS-3) and 290/45 (NiS-4) to reach the same current density. RuO_2, the benchmark OER catalyst, demanded 333 mV to reach 10 mA/cm^2. Ni_3S_2-4, NiS-1, NiS-2, and Ni_3S_2-4, NiS-4 are, therefore, better OER catalysts in terms of overpotential lowering and intrinsic reaction kinetics (Tafel slopes), respectively. Sulfides with relatively larger crystallite sizes tended to show better water splitting activity. For example, the sample with the highest HER performance and the one with the most favorable HER kinetics both fell into the group with larger particle sizes. Notably, surface morphology did not show a clear correlation with performance, as samples with distinct morphologies displayed comparable reaction kinetics. These findings suggest that intrinsic factors, such as crystallinity, conductivity, phase composition, or defect chemistry, may play a more decisive role in determining electrochemical behavior than particle size alone. The OER performance of synthesized nickel sulfides compares well with recently reported similar materials (**Table S4**). The HER and OER results indicate that the synthetic route had no major influence on the sulfide's performance.
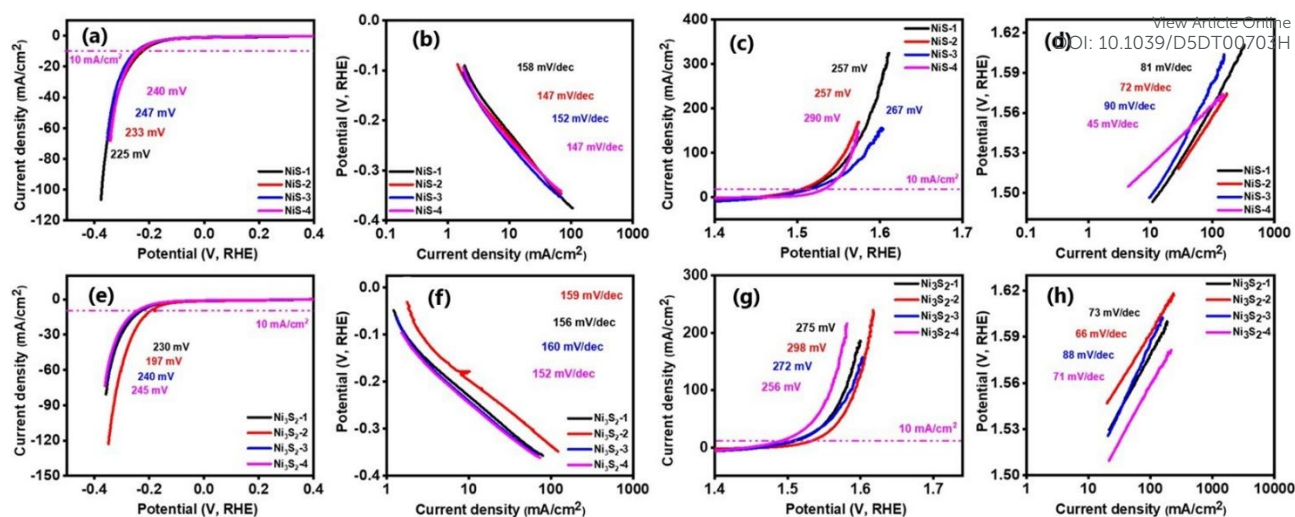
Figure 7. HER polarization curves for (a) NiS, (e) Ni_3S_2 and their corresponding Tafel slopes (b) and (f). OER polarization curves for (c) NiS, (g) Ni_3S_2 and their corresponding Tafel slopes (d) and (h)

The ion diffusion kinetics of an electrode sheds light on its charge/mass transfer processes, which are crucial to its practical application. We, therefore, investigated this property by electrochemical impedance spectroscopy (EIS) measurements. **Figure 8** gives the EIS measurements as Nyquist plots with linear behavior at low frequency and semicircle shape at higher frequency in congruence with other reports.[66] The charge transfer resistance of electroactive species is a function of the semicircle's diameter, with resistance increasing with an increase in diameter.[8, 67] Ni_3S_4-4 showed the lowest charge transfer resistance of 0.6 Ω/cm^2 among all the samples, which correlates with the OER results. Apart from the charge transfer resistance, the stability and ruggedness of an electrode are crucial to its long-term application. The durability of the materials was assessed by employing the polarization curves before and after 1000 CV cycles and long-term chronoamperometry (CA) curves for 24 h. **Figures S10,11** give the HER and OER stability polarization curves of all the electrodes. These curves for the 1st and 1000th cycles matched well indicative of synthesized materials' ruggedness and stability. CA curves for all the nickel sulfides were also employed to probe further into their durability and are given in **Figure S12**. All the sulfides showed good stability of current density over an extended period of 24h with NiS-1, NiS-4 and Ni_3S_4-4 having the best results. The EIS and CA results are suggestive of the feasibility of synthesized nickel sulfides for practical application. The fabricated nickel sulfides have therefore been shown as suitable electrode materials applicable in lowering the constraining energy thermodynamics in HER and OER.
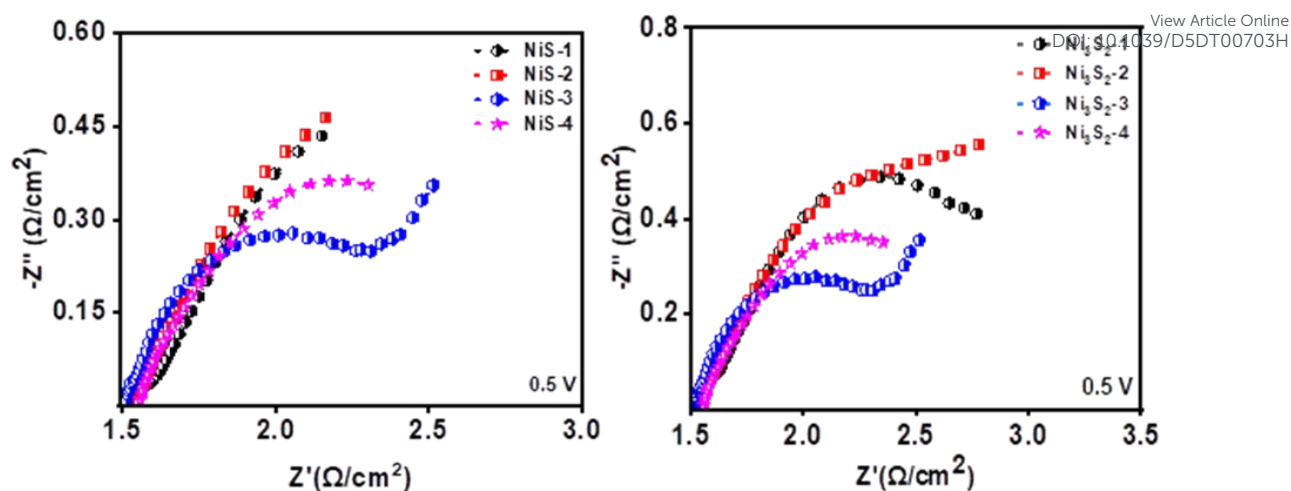
Figure 8. EIS curves of the NiS and Ni_3S_2 electrodes.

Conclusion

Similar phases (NiS and Ni_3S_2) can be prepared via different synthetic routes (colloidal and solvent-less thermolysis) by optimizing the reaction conditions for the thermolysis of metal-organic precursors. The presence of triphenylphosphine (TPP) resulted in the formation of a sulfur-deficient phase (Ni_3S_2), regardless of the precursor and the synthetic route used. The performance of fabricated nickel sulfide electrodes was tested for application in energy storage and energy generation technologies. The Ni_3S_2 prepared by the colloidal route had the best HER performance with an overpotential of 197 mV and a Tafel slope of 159 mV/dec, to attain 10 mA/cm^2 of current density in an alkaline medium. On the contrary, the same phase obtained by the solvent-less route showed the best OER activity. Perhaps the residual carbon from organic moieties on the surface of solventless pyrolyzed Ni_3S_2 negatively affects HER more than OER. Likewise, supercapacitance is also affected by the residual surface carbon, and the best supercapacitance performance was shown by the NiS phase obtained by the decomposition of Ni-Xan in oleylamine. These results indicate careful designing of metal precursors, i.e. precursors that produce volatile by-products or very little residual carbon upon thermolysis. Designing suitable precursors will be a step forward in avoiding surfactants and enhancing the electrochemical performance of electrocatalysts.

Author contributions

G.E. Ayom: conceptualization, data curation, formal analysis, investigation, methodology, writing-original draft; M.D. Khan: validation, visualization, writing-review; R. Srivastava: data curation, writing-original; W. Lin: data curation, writing-original; R. K. Gupta: supervision, writing-review; N. Revaprasadu: funding acquisition, writing-review, supervision.

Data availability

Data generated or analyzed during this study are included in this article and its ESI

Conflict of interest

There are no conflicts to declare.

Acknowledgement:

References

1. T. A. Saleh, *RSC Advances*, 2022, **12**, 23869-23888.
2. P. J. Megía, A. J. Vizcaíno, J. A. Calles and A. Carrero, *Energy & Fuels*, 2021, **35**, 16403-16415.
3. J. Li and S. Jiang, *Global Energy Interconnection*, 2019, **2**, 375-377.
4. M. Kumar, N. K. Singh, K. B. Prajapati, R. S. Kumar and R. Singh, in *Transition Metal-Based Electrocatalysts: Applications in Green Hydrogen Production and Storage*, ACS Publications, 2023, pp. 43-71.
5. R. Tong, M. Xu, Y. Fan, S. Wang, Y. Yuan, H. Huang, C. Zhang and D. Cai, *International Journal of Hydrogen Energy*, 2023, **48**, 3026-3036.
6. Y. Chen, Y. Fan, Z. Cui, H. Huang, D. Cai, J. Zhang, Y. Zhou, M. Xu and R. Tong, *International Journal of Hydrogen Energy*, 2023, **48**, 27992-28017.
7. J. N. Hansen, H. Prats, K. K. Toudahl, N. Mørch Secher, K. Chan, J. Kibsgaard and I. Chorkendorff, *ACS Energy Letters*, 2021, **6**, 1175-1180.
8. G. E. Ayom, M. D. Khan, F. M. de Souza, W. Lin, R. K. Gupta and N. Revaprasadu, *Journal of Energy Storage*, 2024, **97**, 112882.
9. S. Anantharaj, S. Kundu and S. Noda, *Journal of Materials Chemistry A*, 2020, **8**, 4174-4192.
10. G. E. Ayom, M. D. Khan, T. Ingsel, W. Lin, R. K. Gupta, S. J. Zamisa, W. E. van Zyl and N. Revaprasadu, *Chemistry–A European Journal*, 2020, **26**, 2693-2704.
11. C. Manjunatha, N. Srinivasa, S. K. Chaitra, M. Sudeep, R. Chandra Kumar and S. Ashoka, *Materials Today Energy*, 2020, **16**, 100414.
12. X. Zhang, S. Zhu, L. Song, Y. Xu and Y. Wang, *Nanoscale*, 2023, **15**, 3764-3771.
13. S. G. Sibiya, G. E. Ayom, M. D. Khan, J. Choi, S. Bhoyate, R. K. Gupta and N. Revaprasadu, *European Journal of Inorganic Chemistry*, **n/a**, e202300087.

14. G. E. Ayom, M. D. Khan, G. B. Shombe, J. Choi, R. K. Gupta, W. E. van Zyl and N. Revaprasadu, *Inorganic Chemistry*, 2021, **60**, 11374-11384.

15. S. Wang, Z. Geng, S. Bi, Y. Wang, Z. Gao, L. Jin and C. Zhang, *Green Energy & Environment*, 2023.

16. C. Xu, M. Zhang, X. Yin, Q. Gao, S. Jiang, J. Cheng, X. Kong, B. Liu and H.-Q. Peng, *Journal of Materials Chemistry A*, 2023, **11**, 18502-18529.

17. Z. Wang, S. Shen, Z. Lin, W. Tao, Q. Zhang, F. Meng, L. Gu and W. Zhong, *Advanced Functional Materials*, 2022, **32**, 2112832.

18. F. Chen, C. Liu, B. Cui, S. Dou, J. Xu, S. Liu, H. Zhang, Y. Deng, Y. Chen and W. Hu, *Journal of Power Sources*, 2021, **482**, 228910.

19. S. S. Chandraraj and J. R. Xavier, *Surfaces and Interfaces*, 2023, **36**, 102515.

20. Z. H. Tan, X. Y. Kong, B.-J. Ng, H. S. Soo, A. R. Mohamed and S.-P. Chai, *ACS Omega*, 2023.

21. T. Kosmac, D. Maurice and T. H. Courtney, *Journal of the American Ceramic Society*, 1993, **76**, 2345-2352.

22. N. Shaikh, I. Mukhopadhyay and A. Ray, *Journal of Materials Chemistry A*, 2022, **10**, 12733-12746.

23. P. Chen, T. Zhou, M. Zhang, Y. Tong, C. Zhong, N. Zhang, L. Zhang, C. Wu and Y. Xie, *Advanced Materials*, 2017, **29**, 1701584.

24. G. B. Shombe, M. D. Khan, A. M. Alenad, J. Choi, T. Ingsel, R. K. Gupta and N. Revaprasadu, *Sustainable Energy & Fuels*, 2020, **4**, 5132-5143.

25. M. D. Khan, M. Opallo and N. Revaprasadu, *Dalton Transactions*, 2021, **50**, 11347-11359.

26. X. Luo, P. Ji, P. Wang, X. Tan, L. Chen and S. Mu, *Advanced Science*, 2022, **9**, 2104846.

27. H. Liu, J. Cheng, W. He, Y. Li, J. Mao, X. Zheng, C. Chen, C. Cui and Q. Hao, *Applied Catalysis B: Environmental*, 2022, **304**, 120935.

28. Y. Zhang, G. Wang, N. Li, D. Ke and J. Wang, *ChemNanoMat*, 2023, **9**, e202200422.

29. A. Kundu, B. Kumar, A. Rajput and B. Chakraborty, *ACS Applied Materials & Interfaces*, 2023, **15**, 8010-8021.

30. X. Wang, X. Yu, S. Wu, P. He, F. Qin, Y. Yao, J. Bai, G. Yuan and L. Ren, *ACS Applied Materials & Interfaces*, 2023, **15**, 15533-15544.

31. N. Jiang, Q. Tang, M. Sheng, B. You, D.-e. Jiang and Y. Sun, *Catalysis Science & Technology*, 2016, **6**, 1077-1084.

32. S. A. Aladeemy, P. Arunachalam, M. S. Amer and A. M. Al-Mayouf, *RSC advances*, 2025, **15**, 14-25.

33. R. K. Devi, M. Ganesan, T.-W. Chen, S.-M. Chen, M. Akilarasan, S.-P. Rwei, J. Yu, T. Elayappan and A. Shaju, *Journal of Alloys and Compounds*, 2023, **944**, 169261.

34. C. Gervas, S. Mlowe, M. P. Akerman and N. Revaprasadu, *New Journal of Chemistry*, 2018, **42**, 6203-6209.

35. C. Gervas, S. Mlowe, M. P. Akerman, I. Ezekiel, T. Moyo and N. Revaprasadu, *Polyhedron*, 2017, **122**, 16-24.

36. G. B. Shombe, M. D. Khan, C. Zequine, C. Zhao, R. K. Gupta and N. Revaprasadu, *Scientific Reports*, 2020, **10**, 1-14.

37. C. H. DePuy and R. W. King, *Chemical Reviews*, 1960, **60**, 431-457.

38. W. Zhang, Q. Jia, H. Liang, L. Cui, D. Wei and J. Liu, *Chemical Engineering Journal*, 2020, **396**, 125315.

39. T. Kou, T. Smart, B. Yao, I. Chen, D. Thota, Y. Ping and Y. Li, *Advanced Energy Materials*, 2018, **8**, 1703538.

40. Y. Zhao, J. You, L. Wang, W. Bao and R. Yao, *International Journal of Hydrogen Energy*, 2021, **46**, 39146-39182.

41. L. Tian, L. Y. Yep, T. T. Ong, J. Yi, J. Ding and J. J. Vittal, *Crystal Growth and Design*, 2009, **9**, 352-357.

42. A. L. Abdelhady, M. A. Malik, P. O'Brien and F. Tuna, *The Journal of Physical Chemistry C*, 2012, **116**, 2253-2259.

43. A. Roffey, N. Hollingsworth, H.-U. Islam, M. Mercy, G. Sankar, C. R. A. Catlow, G. Hogarth and N. H. de Leeuw, *Nanoscale*, 2016, **8**, 11067-11075.

44. N. Hollingsworth, A. Roffey, H.-U. Islam, M. Mercy, A. Roldan, W. Bras, M. Wolthers, C. R. A. Catlow, G. Sankar and G. Hogarth, *Chemistry of Materials*, 2014, **26**, 6281-6292.

45. M. D. Khan, G. B. Shombe, S. H. Khoza, G. E. Ayom and N. Revaprasadu, *Inorganic Chemistry*, 2024, **63**, 14495-14508.

46. G. E. Ayom, M. D. Khan, J. Choi, R. K. Gupta, W. E. van Zyl and N. Revaprasadu, *Dalton Transactions*, 2021, **50**, 11821-11833.

47. M. D. Khan, G. B. Shombe, S. H. Khoza, G. E. Ayom and N. Revaprasadu, *Inorganic Chemistry*, 2024, DOI: 10.1021/acs.inorgchem.4c01664.

48. M. D. Khan, M. Warczak, G. B. Shombe, N. Revaprasadu and M. Opallo, *Inorganic Chemistry*, 2023, **62**, 8379-8388.

49. Y. Jiang, L. Yuan, Y. Xu, J. Ma, Y. Sun, X. Gao, K. Huang and S. Feng, *Langmuir*, 2019, **35**, 15131-15136.

50. S. Razzaque, M. D. Khan, M. Aamir, M. Sohail, S. Bhoyate, R. K. Gupta, M. Sher, J. Akhtar and N. Revaprasadu, *Inorganic Chemistry*, 2021, **60**, 1449-1461.

51. Y. Li, Y. Bu, X. Chen, T. Zhu, J. Wang, S. Kawi and Q. Zhong, *ChemCatChem*, 2019, **11**, 1320-1327.

52. Y. Chen, J. Meng, M. Xu, L. Qiao, D. Liu, Y. Kong, X. Hu, Q. Liu, M. Chen, S. Lyu, R. Tong and H. Pan, *Advanced Functional Materials*, 2025, **35**, 2413474.

53. R. Geva, N. R. Levy, J. Tzadikov, R. Cohen, M. Weitman, L. Xing, L. Abisdris, J. Barrio, J. Xia and M. Volokh, *Journal of Materials Chemistry A*, 2021, **9**, 27629-27638.

54. B. Guan, Y. Li, B. Yin, K. Liu, D. Wang, H. Zhang and C. Cheng, *Chemical Engineering Journal*, 2017, **308**, 1165-1173.

55. N. Kumar, D. Mishra, S. Y. Kim and S. H. Jin, *Thin Solid Films*, 2020, **709**, 138138.

56. J. S. Chen, Y. Gui and D. J. Blackwood, *Journal of Power Sources*, 2016, **325**, 575-583.

57. Y. Li, K. Ye, K. Cheng, J. Yin, D. Cao and G. Wang, *Journal of Power Sources*, 2015, **274**, 943-950.

58. O. A. González-Meza, E. R. Larios-Durán, A. Gutiérrez-Becerra, N. Casillas, J. I. Escalante and M. Bárcena-Soto, *Journal of Solid State Electrochemistry*, 2019, **23**, 3123-3133.

59. J. S. Ko, M. B. Sassin, D. R. Rolison and J. W. Long, *Electrochimica Acta*, 2018, **275**, 225-235.

60. V. Kushwaha, K. D. Mandal, A. Gupta and P. Singh, *Dalton Transactions*, 2024, **53**, 5435-5452.

61. N. Kumar, D. Mishra and S. Y. Kim, *Thin Solid Films*, 2020, **709**, 138138.

62. J. S. Chen, C. Guan, Y. Gui and D. J. Blackwood, *ACS Applied Materials & Interfaces*, 2017, **9**, 496-504.

63. B. J. Reddy, P. Vickraman and A. S. Justin, *Journal of Materials Science*, 2019, **54**, 6361-6373.

64. Y. Dong, G. Zhang, Q. Liu, C. Qi, X. Jiang and D. Gao, *Journal of Alloys and Compounds*, 2022, **923**, 166438.

65. C. Liu, D. Jia, Q. Hao, X. Zheng, Y. Li, C. Tang, H. Liu, J. Zhang and X. Zheng, *ACS Applied Materials & Interfaces*, 2019, **11**, 27667-27676.

66. M. Kong, Z. Wang, W. Wang, M. Ma, D. Liu, S. Hao, R. Kong, G. Du, A. M. Asiri and Y. Yao, *Chemistry–A European Journal*, 2017, **23**, 4435-4441.

67. G. E. Ayom, M. D. Khan, S. C. Masikane, F. M. de Souza, W. Lin, R. K. Gupta and N. Revaprasadu, *Sustainable Energy & Fuels*, 2022, **6**, 1319-1331.

Data availability

Data generated or analyzed during this study are included in this article and its ESI